EFFICIENT COMPUTATION OF REGULARIZED FIELD MAP ESTIMATES IN 3D

Greg Ongie, Junyun Shi, Jeffrey A. Fessler

University of Michigan, EECS and BME Departments, Ann Arbor, MI, USA

ABSTRACT

Estimating the main magnetic field inhomogeneity is important for many magnetic resonance imaging (MRI) techniques. Regularized estimation methods can provide accurate estimates that intrinsically avoid phase wrapping, account for the chemical shift due to fat, and reduce noise. However, these methods require minimizing nonconvex cost functions and existing algorithms are undesirably slow or do not scale to realistic 3D datasets due to memory limitations. This paper proposes a new algorithm that overcomes these limitations. The algorithm adapts the nonlinear conjugate gradient method by incorporating an monotonic line search and efficient iteration-dependent preconditioning. Experiments on multi-echo field map estimation show that our algorithm is competitive with state-of-the-art methods in 2D, and scale successfully to 3D datasets, where current fast methods fail due to memory limitations.

***Index Terms*—** Field inhomogeneity, field map estimation, water-fat imaging, nonlinear conjugate gradient method

1. INTRODUCTION

Inhomogeneities within the main magnetic field ($\boldsymbol{B}_0$) can degrade magnetic resonance imaging (MRI) techniques that use long readout times (e.g., spiral trajectories or echo planar imaging). Field inhomogeneity is also a nuisance parameter in chemical shift based water-fat imaging techniques [1]. However, accurate estimates of the off-resonance frequency induced by the field inhomogeneity at each voxel (i.e., a field map) can mitigate both of these issues.

Numerous methods have been proposed to estimate field maps. One approach is to acquire multiple scans at different echo times and then estimate the field inhomogeneity from the phase information in the resulting images [1]. Alternatively, regularized estimation methods such as [2, 3] estimate a smooth field map from multiple acquisition images while intrinsically accounting for phase wrapping. The challenge with these regularized methods is that they use nonconvex cost functions that require iterative minimization techniques.

An existing minimization technique for regularized field map estimation uses optimization transfer to create a separable quadratic surrogate (SQS) [2]. However, that method takes many iterations, and subsequently a long time, to reach a useful solution. This large computational cost impedes the adoption of these estimators, especially for 3D datasets.

This paper presents a new method that significantly decreases the computation time (or memory demands) of regularized field map estimators. The new method builds off a recent approach [4] that uses Huber's algorithm for quadratic surrogates [5] by exploiting the structure of the Hessian matrix of the quadratic surrogate function. In [4], a Cholesky decomposition provides fast inversion of the Hessian matrix by exploiting its banded structure that arises from finite difference regularization. However, this approach does not scale to full 3D volumes with 3D regularization because of the increase in size and bandwidth of the Hessian matrix.

Instead, this paper adapts the nonlinear conjugate gradient algorithm combined with a monotonic line search approach and efficiently obtained iteration-dependent preconditioners. In particular, we derive an effective preconditioner from an incomplete Cholesky decomposition of an approximation of the Hessian. Results with simulated and *in vivo* data demonstrate that the new algorithm is competitive with the method in [4] on smaller datasets, and scales to 3D datasets where the approach of [4] is infeasible due to memory limitations. In brief, the proposed algorithm enables fast and memory efficient regularized field map estimates, even for 3D volumes.

2. PROBLEM FORMULATION

Let $y_{\ell,j} \in \mathbb{C}$ denote the jth voxel in the reconstructed image of the ℓth scan, for $j = 1, \ldots, N$ and $\ell = 1, \ldots, L$. We model the effect of field inhomogeneity as [2]:

$$y_{\ell,j} = e^{i\omega_j t_\ell} x_j + \varepsilon_{\ell,j} \tag{1}$$

where $x_j \in \mathbb{C}$ denotes the unknown magnetization at the jth voxel, $\omega_j \in \mathbb{R}$ denotes the field map value at voxel j, t_ℓ denotes the echo time shift of the ℓth scan, and $\varepsilon_{\ell,j} \in \mathbb{C}$ denotes the complex noise. For simplicity, this paper neglects the effect of R_2^* decay; however, one can incorporate that effect into the model (1) and the derivations easily [2].

Assuming the noise $\varepsilon_{\ell,j}$ is zero-mean, white complex Gaussian, the joint maximum-likelihood (ML) estimates of the field map vector $\boldsymbol{\omega}$ and image vector $\boldsymbol{x}$ are given by

$$\arg\min_{\boldsymbol{\omega},\boldsymbol{x}} \sum_{j=1}^{N} \sum_{\ell=1}^{L} \left| y_{\ell,j} - e^{i\omega_j t_\ell} x_j \right|^2 . \tag{2}$$

Supported in part by NIH grants P01 CA059827 and R01 EB023618.

978-1-5090-1172-8/17/$31.00 ©2017 IEEE

For a given field map $\boldsymbol{\omega}$, the ML estimate of $\boldsymbol{x}$ from (2) has an analytic solution. Substituting that solution back into (2) and simplifying gives the following negative log-likelihood for multi-echo field map estimation [2]:

$$\Phi_F(\boldsymbol{\omega}) \triangleq \sum_{j=1}^{N} \sum_{m=1}^{L} \sum_{p=1}^{L} \varphi_{jmp}(\omega_j) \tag{3}$$

where, with weighting $w_j^{m,p} = |y_{m,j} y_{p,j}|^2 / \sum_{\ell=1}^{L} |y_{\ell,j}|^2$:

$$\varphi_{jmp}(\omega_j) = w_j^{m,p} \left[1 - \cos(\omega_j(t_m - t_p) + \angle y_j^m - \angle y_{p,j})\right]. \tag{4}$$

Field maps tend to be smooth within body tissue [2], therefore a spatial regularizing term is combined with the log-likelihood to define a penalized-likelihood (PL) estimator [2]. Furthermore, field map estimates are only needed for voxels where signal is present, hence we incorporate an estimation mask yielding the final generalized PL cost function:

$$\Psi(\boldsymbol{\omega}_\mathrm{s}) = \Phi(\boldsymbol{\omega}_\mathrm{s}) + \frac{\beta}{2} \|\boldsymbol{C}\boldsymbol{\omega}_\mathrm{s}\|_2^2, \tag{5}$$

$$\Phi(\boldsymbol{\omega}_\mathrm{s}) \triangleq \sum_{j \in \mathcal{N}_\mathrm{s}} \sum_{m=1}^{L} \sum_{p=1}^{L} \varphi_{jmp}(\omega_j),$$

where $\boldsymbol{\omega}_\mathrm{s} \in \mathbb{R}^{|\mathcal{N}_\mathrm{s}|}$ is a vector containing the field map variables within the estimation mask, $\mathcal{N}_\mathrm{s}$ is the set of voxels within the mask, β is a regularization parameter, and $\boldsymbol{C}$ is a finite differencing matrix that accounts for the mask.

Estimators based on minimizing this cost function provide accurate field map estimates [2]; however, the cost function is difficult to minimize due to the nonlinear data-fit terms and the non-separability of the regularizer. Current minimization strategies that use separable quadratic surrogate methods that can take many minutes to converge even for 2D images [2], or are limited to small data sizes because of memory limitations [4]. The next section proposes a new minimization strategy that reduces both the computation time and memory demands.

3. PROPOSED ALGORITHM

We propose a method based on the nonlinear conjugate gradient (NCG) algorithm as applied to the PL cost function (5). In particular, we adapt the following preconditioned form of the Polak-Ribiere NCG method:

$$\begin{aligned}
\boldsymbol{g}^n &= \nabla \Psi(\boldsymbol{\omega}_\mathrm{s}^n) && \text{(gradient)} \\
\boldsymbol{p}^n &= \boldsymbol{P}^{-1} \boldsymbol{g}^n && \text{(precondition)} \\
\gamma_n &= \begin{cases} 0, & n = 0 \\ \frac{\langle \boldsymbol{g}^n - \boldsymbol{g}^{n-1}, \boldsymbol{p}^n \rangle}{\langle \boldsymbol{g}^{n-1}, \boldsymbol{p}^{n-1} \rangle}, & n > 0 \end{cases} \\
\boldsymbol{z}^n &= \boldsymbol{p}^n + \gamma_n \boldsymbol{z}^{n-1} && \text{(search direction)} \\
\alpha_n &= \arg\min_\alpha \Psi(\boldsymbol{\omega}_\mathrm{s}^n + \alpha \boldsymbol{z}^n) && \text{(step size) (6)} \\
\boldsymbol{\omega}_\mathrm{s}^{n+1} &= \boldsymbol{\omega}_\mathrm{s}^n + \alpha_n \boldsymbol{z}^n && \text{(update)}
\end{aligned}$$

We alter the NCG method by considering two modifications. First, we derive a monotonic step size line search algorithm using quadratic surrogates like in [6]. Second, we consider several preconditioners based on quadratic majorizers.

3.1. Monotonic step size line search

The non-quadratic nature of the cost function (5) prevents direct computation of a step size. Instead, we must consider iterative line search methods. There are many existing line search methods capable of determining a "sufficient" step size [7]. The disadvantage of many of these methods is that they require multiple costly evaluations of the cost function and they have parameter values that would have to be carefully selected for such nonconvex problems. Instead, we follow [6] and use a line search method based on Huber's algorithm for quadratic surrogates [5]. This particular line search method is guaranteed to monotonically decrease the cost function.

To create the monotonic line search algorithm, we evaluate the original cost function (5) with respect to a scalar step size variable, α (dropping outer iteration n for brevity):

$$f(\alpha) = \Phi(\boldsymbol{\omega}_\mathrm{s} + \alpha \boldsymbol{z}) + \frac{\beta}{2} \|\boldsymbol{C}(\boldsymbol{\omega}_\mathrm{s} + \alpha \boldsymbol{z})\|_2^2, \tag{7}$$

where $\boldsymbol{z} \in \mathbb{R}^{|\mathcal{N}_\mathrm{s}|}$ is a search direction. The optimal step size in (7) corresponds to solving

$$\alpha^* = \arg\min_\alpha f(\alpha).$$

However, minimizing f directly is intractable due to the nonlinear data fit term. Instead, we adapt Huber's method of quadratic surrogates [5,6] and iteratively minimize f by minimizing a sequence of 1-D surrogate functions q_k:

$$\alpha^{(k+1)} = \arg\min_\alpha \ q_k(\alpha). \tag{8}$$

Here the surrogate functions q_k are given by

$$\begin{aligned} q_k(\alpha) \triangleq{}& \Phi(\boldsymbol{\omega}_\mathrm{s} + \alpha^{(k)} \boldsymbol{z}) + \boldsymbol{z}^\mathrm{T} \nabla \Phi(\boldsymbol{\omega}_\mathrm{s} + \alpha^{(k)} \boldsymbol{z})(\alpha - \alpha^{(k)}) \\ &+ \frac{1}{2} d^{(k)} (\alpha - \alpha^{(k)})^2 + \frac{\beta}{2} \|\boldsymbol{C}(\boldsymbol{\omega}_\mathrm{s} + \alpha \boldsymbol{z})\|_2^2, \end{aligned} \tag{9}$$

where $d^{(k)} = \sum_{j \in \mathcal{N}_\mathrm{s}} |z_j|^2 d_j^{(k)}$ with

$$d_j^{(k)} = \sum_{m=1}^{L} \sum_{p=1}^{L} \kappa_{jmp} \left(s_{jmp}(\omega_j + \alpha^{(k)} z_j) \right), \tag{10}$$

and where

$$\kappa_{jmp}(s) \triangleq w_j^{m,p} (t_m - t_p)^2 \frac{\sin(s)}{s}, \tag{11}$$

$$s_{jmp}(\omega) \triangleq \left(\omega \cdot (t_m - t_p) + \angle y_j^m - \angle y_{p,j} \right) \bmod \pi, \tag{12}$$

are the optimal Huber's curvatures [2, 5]. Minimizing the quadratic (9) yields the following updates:

$$\alpha^{(k+1)} = \alpha^{(k)} - \frac{\frac{\partial}{\partial \alpha} f(\alpha^{(k)})}{d_\alpha^{(k)} + \beta \boldsymbol{z}^{\mathrm{T}} \boldsymbol{C}^{\mathrm{T}} \boldsymbol{C} \boldsymbol{z}}. \tag{13}$$

The above choice of surrogate function q_k is designed to majorize f in the sense that $q_k(\alpha) \geq f(\alpha)$, for all α and for all subiterations k. From this property it can be shown that the sequence of $\alpha^{(k)}$ monotonically decreases the cost function (7). Also note that we implement the iterates (13) efficiently by computing $\beta \boldsymbol{z}^{\mathrm{T}} \boldsymbol{C}^{\mathrm{T}} \boldsymbol{C} \boldsymbol{z}$ only once per outer iteration.

3.2. Preconditioning matrices

We also explore several preconditioners to accelerate our NCG based algorithm. We base our preconditioners on the following iteration dependent approximation of the Hessian:

$$\boldsymbol{H}_n \triangleq \boldsymbol{D}_n + \beta \boldsymbol{C}^T \boldsymbol{C}$$

where $\boldsymbol{D}_n = \mathrm{diag}(d_j^{(K_n)})$ with K_n denoting the final line search step in the $(n-1)$th iteration of the NCG algorithm. This approach is more efficient than re-computing the exact Hessian of the original cost function (5), because we obtain $\boldsymbol{H}_n$ as a by-product of the line search.

Our first preconditioning matrix restricts $\boldsymbol{H}_n$ to its diagonal entries: $\boldsymbol{P}_{\mathrm{D}} = \mathrm{diag}(\boldsymbol{H}_n)$. Our second preconditioner is the full Hessian matrix of the quadratic surrogate $\boldsymbol{P}_{\mathrm{H}} = \boldsymbol{H}_n$ which is implemented using sparse Cholesky factorization. However, the sparse Cholesky factorization is infeasible for large 3D datasets due to memory demands. Therefore, we also consider an incomplete Cholesky decomposition [8] as a preconditioner, which has the form $\boldsymbol{P}_{\mathrm{I}} = \boldsymbol{K}\boldsymbol{K}^T \approx \boldsymbol{H}_n$, where $\boldsymbol{K}$ is a sparse lower triangular matrix. We note that the incomplete Cholesky decomposition is substantially less computationally demanding and memory intensive than a full Cholesky decomposition, and scales well to large 3D datasets.

4. RESULTS

We performed field map estimation using our NCG with monotonic line search algorithm with no preconditioner (NCG-MLS), with the diagonal preconditioner (NCG-MLS-D), with the Hessian preconditioner based on a Cholesky decomposition (NCG-MLS-C), and an incomplete Cholesky decomposition (NCG-MLS-IC). We also compared with the existing SQS algorithm [2] and quadratic surrogate Huber's algorithm [4] (QS-Huber). We used one line search iteration for NCG-MLS, NCG-MLS-D, NCG-MLS-IC, and three for NCG-MLS-C. These parameter values were determined empirically in advance and were not further optimized.

We initialized each algorithm using a tightly masked conventional estimate. The conventional method takes the phase difference of the first two acquired images as follows [2]:

$$\hat{\omega}_j^{\mathrm{conv}} = \angle \left(y_{1,j}{}^* y_{2,j} \right) / t_1. \tag{14}$$

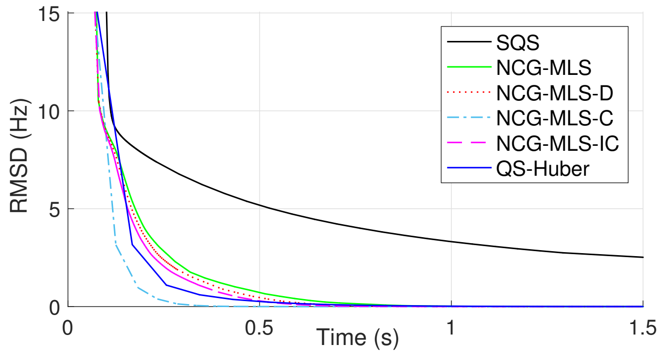

Fig. 1. Plots of the RMSD in Hz versus time for all of the algorithms evaluated on a simulated 2D dataset. The proposed family of NCG-MLS algorithms are comparable in computation time to the state-of-the-art QS-Huber method [4].

With this initialization we observed all of the algorithms considered converged to the same solution to within machine precision in the experiments carried out in this work. Hence, we compared convergence rates by computing the root-mean squared difference (RMSD) between the estimate at each iteration $\boldsymbol{\omega}_{\mathrm{s}}^n$ and the mean of the final estimates from the SQS method and the NCG-MLS method $\hat{\boldsymbol{\omega}}_{\mathrm{s}}$, where $\mathrm{RMSD}(\boldsymbol{\omega}_{\mathrm{s}}^n) = \sqrt{\|\boldsymbol{\omega}_{\mathrm{s}}^n - \hat{\boldsymbol{\omega}}_{\mathrm{s}}\|_2^2} / \sqrt{|\mathcal{N}_{\mathrm{s}}|}$. Comparing against the mean of two estimates avoids favoring any one algorithm. We implemented all algorithms in MATLAB and ran the experiments on a PC with a dual 6-core 2.80GHz Intel Xeon CPU and 32 GB of RAM.

We first tested our algorithms on a partially simulated multi-echo dataset of a 128×128 pixel brain image and field map acquired on a 3T GE scanner (not pictured). The original data was collected at two echo times 2 ms apart, from which we estimated the field map and the brain image, which we took as ground truth. From the ground truth field map and brain image we simulated a 3-echo acquisition with relative echo times $t_\ell = 0, 2, 10\,\mathrm{ms}$ and $R_2^* = 20\,\mathrm{s}^{-1}$. We added complex Gaussian noise to these images so that the SNR $\approx 20\,\mathrm{dB}$. We used second-order finite differences in the definition of $\boldsymbol{C}$, which we found to give improved results over first-order differences. We selected the regularization parameter $\beta = 2^{-3}$ as it provided the most accurate estimates compared to the truth (details not shown). Fig. 1 plots RMSD in Hz versus wall time for all of the evaluated methods. The family of NCG-MLS methods converged at a rate similar to the QS-Huber method in this case, with NCG-MLS-C converging the fastest.

We also investigated an *in vivo* 3D MRI dataset ($64 \times 64 \times 40$ voxels) collected at two echo times 2.3 ms apart; see Fig. 2 for nine representative slices. For this dataset, we

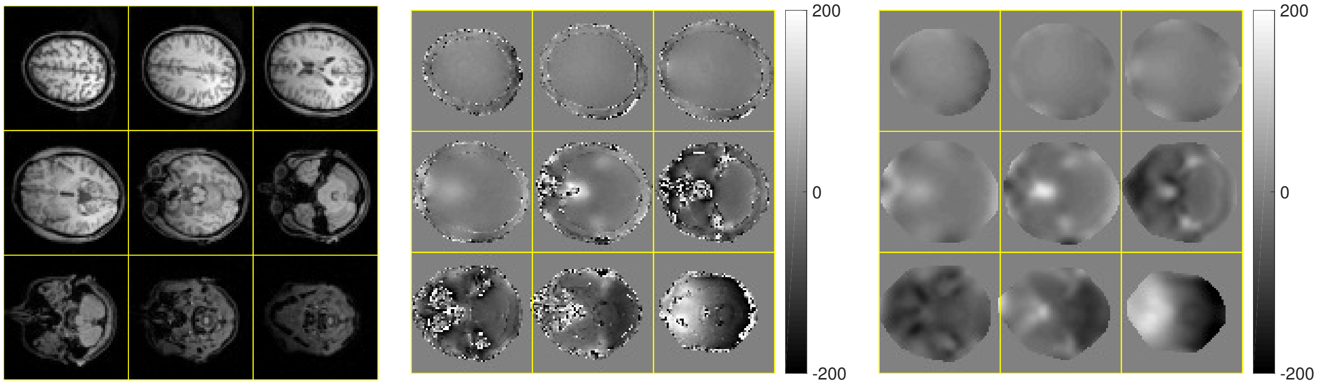

Fig. 2. Representative slices of a 3D brain dataset used in experiments: (left) magnitude image for reference, (middle) initial field map estimate in Hz, and (right) regularized field map estimate in Hz.

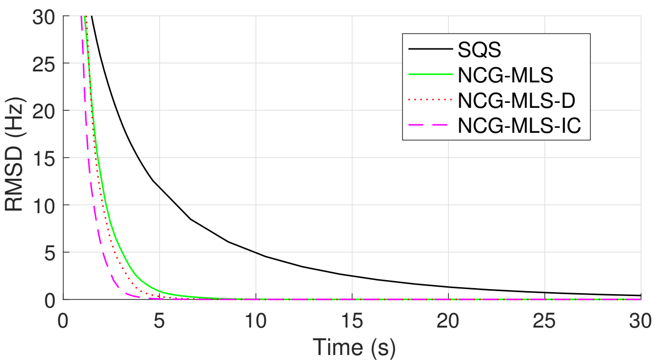

Fig. 3. Plots of RMSD in Hz versus time for all of the algorithms evaluated on the 3D brain dataset. The QS-Huber method [4] was infeasible in this setting due to memory limitations.

could not apply the QS-Huber and NCG-MLS-C methods due to memory limitations, and so do not compare against these methods. We reused the the same parameter settings as in the 2D setting, and extended $\boldsymbol{C}$ to include second-order finite differences in the axial dimension. Fig. 3 shows RMSD in Hz versus time for all of the evaluated methods. This case also exhibited similar improvement in the convergence rates with NCG-MLS over SQS. The preconditioned methods NCG-MLS-D and NCG-MLS-IC showed modest improvement over NCG-MLS without preconditioning.

5. DISCUSSION AND CONCLUSION

We have presented a efficient method for minimizing the non-convex cost function associated with regularized field map estimation. The method modifies the nonlinear conjugate gradient method by including a monotonic step size line search algorithm based on a quadratic surrogate. Our fastest algorithms were those that used the additional preconditioning based on an approximation of the Hessian. These converged to the same estimate as the existing separable quadratic surrogate method an order of magnitude faster and show similar convergence speedups on full 3D volumes, where existing fast methods are infeasible due to memory limitations.

Acknowledgment: We thank Jon-Fredrik Nielsen at the Univ. of Michigan for the multi-echo 3D MRI brain scan data.

6. REFERENCES

[1] T. A. Bley, O. Wieben, C. J. Francois, J. H. Brittain, and S. B. Reeder, "Fat and water magnetic resonance imaging," *J. Mag. Res. Im.*, vol. 31, no. 1, pp. 4–18, Jan. 2010.

[2] A. K. Funai, J. A. Fessler, D. T. B. Yeo, V. T. Olafsson, and D. C. Noll, "Regularized field map estimation in MRI," *IEEE Trans. Med. Imag.*, vol. 27, no. 10, pp. 1484–94, Oct. 2008.

[3] D. Hernando, J. P. Haldar, B. P. Sutton, J. Ma, P. Kellman, and Z-P. Liang, "Joint estimation of water/fat images and field inhomogeneity map," *Mag. Res. Med.*, vol. 59, no. 3, pp. 571–80, Mar. 2008.

[4] M. J. Allison and J. A. Fessler, "Accelerated computation of regularized field map estimates," in *Proc. Intl. Soc. Mag. Res. Med.*, 2012, p. 0413.

[5] P. J. Huber, *Robust statistics*, Wiley, New York, 1981.

[6] J. A. Fessler and S. D. Booth, "Conjugate-gradient preconditioning methods for shift-variant PET image reconstruction," *IEEE Trans. Im. Proc.*, vol. 8, no. 5, pp. 688–99, May 1999.

[7] C. T. Kelley, *Iterative methods for optimization*, Soc. Indust. Appl. Math., 1999.

[8] T. A. Manteuffel, "An incomplete factorization technique for positive definite linear systems," *Mathematics of Computation*, vol. 34, no. 150, pp. 473–97, Apr. 1980.